Geological Society of America Bulletin

Enhanced fracture permeability and accompanying fluid flow in the footwall of a normal fault: The Hurricane fault at Pah Tempe hot springs, Washington County, Utah

Stephen T. Nelson, Alan L. Mayo, Stuart Gilfillan, Sarah J. Dutson, Ronald A. Harris, Zoe K. Shipton and David G. Tingey

Geological Society of America Bulletin 2009;121;236-246
doi:10.1130/B26285.1

Notes

Enhanced fracture permeability and accompanying fluid flow in the footwall of a normal fault: The Hurricane fault at Pah Tempe hot springs, Washington County, Utah

Stephen T. Nelson†
Alan L. Mayo
Department of Geological Sciences, Brigham Young University, S-389 ESC, Provo, Utah 84602, USA

Stuart Gilfillan
School of Geosciences, Grant Institute of Geology, The King's Buildings, West Mains Road, Edinburgh EH9 3JW, UK

Sarah J. Dutson
Ronald A. Harris
Department of Geological Sciences, Brigham Young University, S-389 ESC, Provo, Utah 84602, USA

Zoe K. Shipton
Department of Geographical and Earth Sciences, Glasgow University, Gregory Building, Lilybank Gardens, Glasgow G12 8QQ, UK

David G. Tingey
Department of Geological Sciences, Brigham Young University, S-389 ESC, Provo, Utah 84602, USA

ABSTRACT

The Pah Tempe hot springs discharge ~260 L/s of water at ~40 °C into the Virgin River in the footwall damage zone of the Hurricane fault at Timpoweap Canyon, near Hurricane, Utah, USA. Although these are Na-Cl waters, they actively discharge CO_2 gas and contain significant quantities of CO_2 (~34.6 mmol/kg), predominantly as H_2CO_3 and HCO_3^-. Because of excellent exposures, Pah Tempe provides an exceptional opportunity to observe the effects of enhanced fracture permeability in an active extensional fault.

Pah Tempe waters have been deeply circulated (>5 km; >150 °C) into basement rock as illustrated by the clear water-rock exchange of oxygen isotopes. Waters were probably recharged under colder climate conditions than present and therefore have a prolonged subsurface residence. Discharge of both water and gas in the springs correlates to the density of fractures in carbonate rocks above stream level. This observation suggests that clusters of high fracture density in the fault-damage zone act as pathways from the likely regional aquifer, the eolian Queantoweap Sandstone, through the overlying confining unit, the gypsiferous silty Seligman Member of the Kaibab Formation.

Mass-balance modeling suggests that the majority of CO_2 discharge is the product of the quantitative dissolution of CO_2 gas at depth within the fault zone. Upon discharge, most of the carbon is released to the surface as dissolved species. It appears that the subsurface production rate of CO_2 is relatively low because Pah Tempe waters are grossly undersaturated in CO_2 at inferred minimum circulation depths and temperatures. Geological and geochemical data also suggest that the CO_2 is dominated by a crustal component complemented by minor mantle contributions.

Keywords: hydrogeology, CO_2 flux, damage zone, aqueous geochemistry, structural geology.

INTRODUCTION

The role of enhanced permeability in fault zones in enabling the deep circulation of fluids is an important topic that merges hydrogeology, structural geology, and geochemistry. The flow of a number of different types of fluids may be enhanced at fault zones, including: oil and natural gas, groundwater, ore-bearing fluids, and magmas. Of recent interest is the geologic sequestration of CO_2 (e.g., IPCC, 2005), and faults are one means by which natural or artificial CO_2 reservoirs could fail (Benson and Hepple, 2005; Shipton et al., 2005a).

The Hurricane fault near St. George, Utah (Fig. 1), is an example where the active discharge of water and CO_2 can be examined in detail. In particular, discharge from nearly horizontal subsurface sedimentary sequences that include clastic and carbonate rocks of variable primary permeability is accommodated through the footwall of a major extensional fault and its related damage zone. Thus, the purpose of this paper is to summarize and describe the setting of fluid discharge, to provide a preliminary assessment of the origin and flux rate of water and CO_2 discharge, and to examine the enhanced permeability in the footwall of this major normal fault.

Hydrogeologic Setting

The Hurricane fault is an active, steeply west-dipping normal fault that separates the Colorado Plateau from the Basin and Range Province (Stewart et al., 1997; Taylor et al., 2001) (Fig. 1). Where the Virgin River crosses the fault, just north of Hurricane, Utah, it has deeply incised the Permian Kaibab and Toroweap Formations. The local arid climate limits vegetative cover such that there is near complete exposure of ~200 m of rock in the canyon walls, revealing exposures of the ≥500-m-wide footwall damage zone (Fig. 2). At this location, known locally as

†E-mail: stn@geology.byu.edu

GSA Bulletin; January/February 2009; v. 121; no. 1/2; p. 236–246; doi: 10.1130/B26285.1; 9 figures; 4 tables.

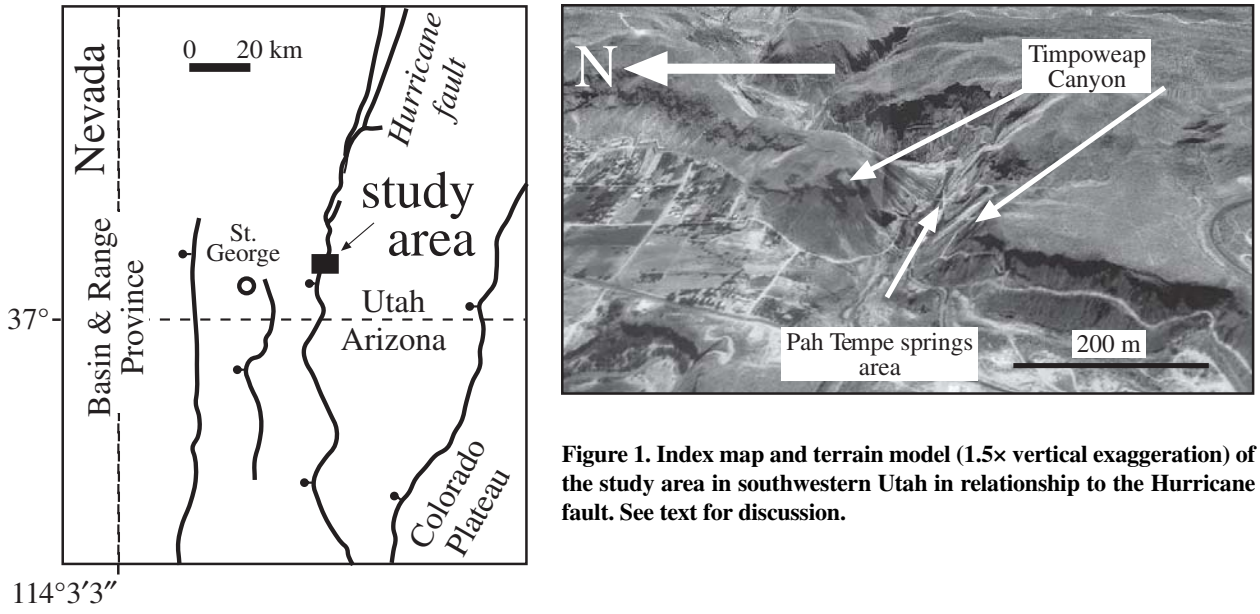

Figure 1. Index map and terrain model (1.5× vertical exaggeration) of the study area in southwestern Utah in relationship to the Hurricane fault. See text for discussion.

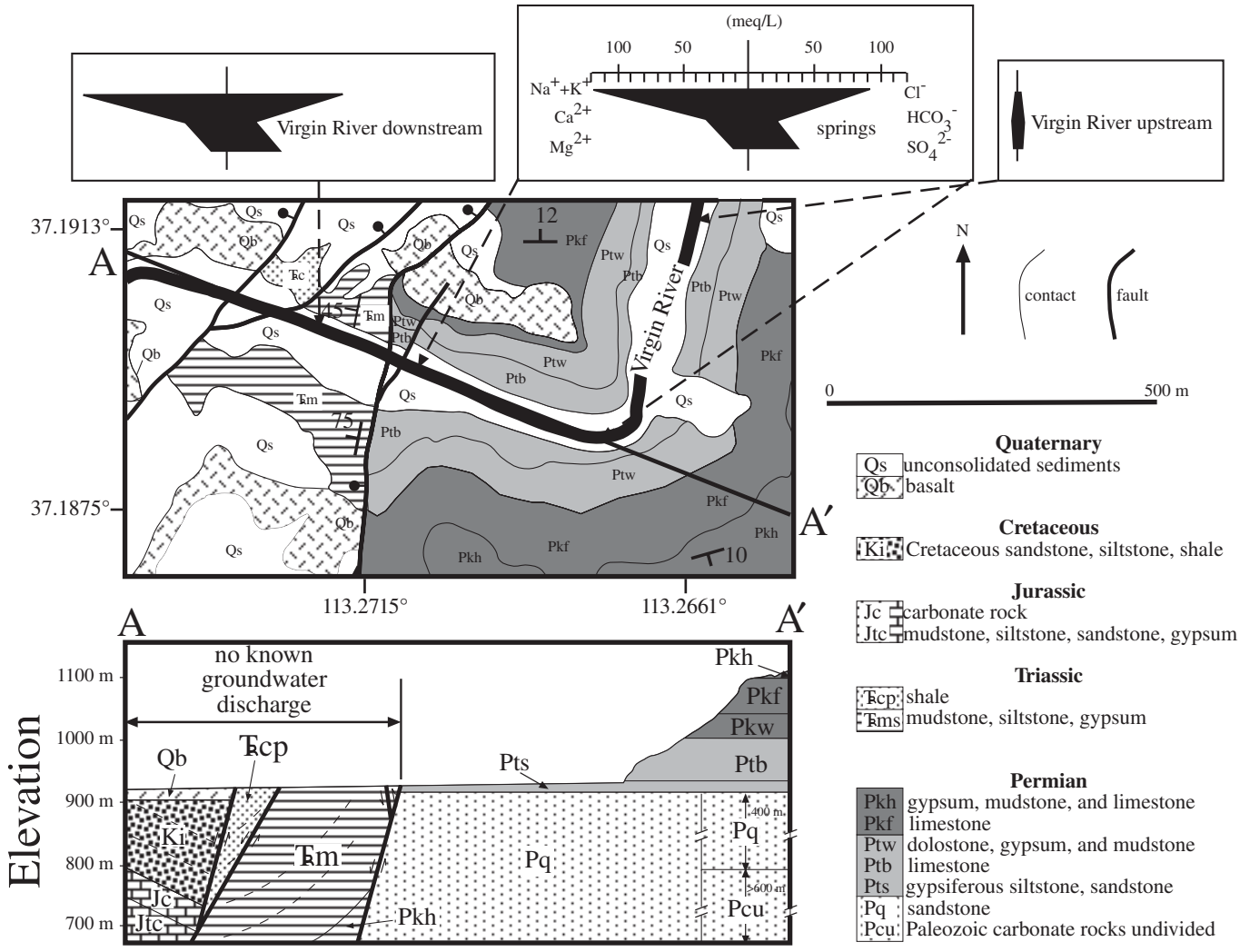

Figure 2. Simplified geologic map (after Biek, 2003) and cross section of the Pah Tempe area. Stiff diagrams have been added to the geologic map to indicate changes in water quality due to spring discharge. Stiff diagram scale applies to all three waters.

Pah Tempe or Dixie hot springs, large quantities of thermal water (~40 °C, 260 L/s; Dutson, 2005) discharge at, or as much as, 2–3 m above stream level within the footwall damage zone of the fault. As will be shown here, large quantities of CO_2 (both exsolved, actively exsolving, and dissolved) are released here. Dissolved CO_2 is represented by elevated bicarbonate and carbonic acid contents of the water. Exsolved CO_2, by contrast, is represented by large numbers of bubble trains of nearly pure CO_2 rising through the streambed, whereas passively exsolving CO_2 (without bubbles) can be detected immediately above the surface of spring pools.

Although a fair amount of work relevant to the Hurricane fault has been conducted, relatively little detailed work has been done at the Pah Tempe locality until recently. Biek (2003) mapped the 7.5′ quadrangle that contains the site, and Lund et al. (2002) summarized the slip history and geometry of the fault (2370 m total throw and 0.2 mm/yr slip) at Pah Tempe. Dutson (2005) provided the chief detailed study on the hydrogeology of spring discharge.

It is not surprising that spring discharge takes place at Pah Tempe. Low-permeability mudstones (Moenkopi Formation) are juxtaposed across the fault in the hanging wall (Fig. 2), downcutting of the Virgin River provides a regional topographic low, and the damage zone of the fault provides fracture permeability for the migration of fluids. Above stream level, the Toroweap and Kaibab Formations are composed of intercalated members of cliff-forming carbonate rock and slope-forming siltstones that are locally gypsiferous. Downcutting has brought the stream in contact with the 10–15-m-thick gypsiferous siltstone Seligman Member (unit Pts) of the Toroweap Formation (unit Pt, Fig. 2).

Due to its fine-grained and gypsiferous nature, the Seligman Member should be relatively impermeable and sustain open fractures poorly relative to massive overlying and underlying units. Beneath the Seligman Member, there is the thick, massive, and competent eolian Queantoweap Sandstone (unit Pq, Fig. 2), which likely exhibits substantial primary porosity and permeability, as well as secondary fracture permeability in less porous units. Beneath this unit, there is a substantial thickness of sedimentary rocks dominated by carbonate rocks in which the permeability is dominated by fractures that may be accompanied by solution weathering (Fig. 3). Thus, the Seligman Member could act as a cap on subjacent hydrostratigraphic units, whereas the Queantoweap Formation and units below it accommodate far-field flow.

Methods

Anion concentrations other than bicarbonate (measured by titration) were determined at Brigham Young University (BYU) using a Dionex ICS-90 ion chromatograph. Cation abundances were measured with a Perkin Elmer 5100C Atomic Absorption Spectrometer. The acceptable charge balance error was ≤5%.

Stable isotope ratios $\delta^{18}O_{VSMOW}$ and δD_{VSMOW} were measured at BYU with a Finnigan Delta^{plus} isotope-ratio mass spectrometer using methods similar to Epstein and Mayeda (1953) and Gehre et al. (1996), and values were normalized to the Vienna standard mean ocean water (VSMOW)/standard light Antarctic precipitation (SLAP) scale (Coplen, 1988; Nelson, 2000; Nelson and Dettman, 2001). One dissolved inorganic carbon (DIC) sample, quantitatively precipitated as $BaCO_3$ and acidified (McCrea, 1950), and one exsolved CO_2 gas sample were analyzed at BYU against an NBS-19 calibrated reference gas. Two exsolved CO_2 gas samples were measured at Scottish Universities Environmental Research Centre (SUERC), East Kilbride. Typical uncertainties were ±1‰ for δD, ±0.3‰ for $\delta^{18}O$, and ±0.2‰ for $\delta^{13}C$.

One spring sample analyzed for tritium (^3H; below detection limit) was prepared similar to the method of the University of Waterloo Environmental Isotope Laboratory (Drimmie et al., 1993) and analyzed at BYU with a Perkin Elmer Quantulus 1220 Liquid Scintillation Counter (LSC). Gas samples analyzed for CO_2 and helium isotopes were measured by mass spectrometry at the University of Utah following collection in well-purged and crimped Cu-tubing (e.g., Hendry et al., 2005).

Both the number of gas-vent outflows and the volume of gas released were estimated by counts conducted on a single day. The bed of the Virgin River was divided into 6.1 m intervals, and bubble trains in each interval were counted by three separate individuals, permitting the estimation of a mean bubble train count for each 6.1 m section. Intervals extended from the eastern trace of the Hurricane fault to ~525 m upstream, the location of the last observed gas vents, thereby defining the width of the damage zone in terms of gas discharge. The volumes of selected gas-vent outflows along the streambed were averaged for 10 gas vents using a funnel and a 50 mL container. The container and funnel were filled with water and then placed over the gas outflows, and the time for the water to be displaced by gas was recorded. Atmospheric CO_2 concentrations were measured with a portable Vaisala meter.

Gain-loss flow measurements of the Virgin River were made during low-flow periods using a Flo-Mate portable flow meter. Flow measurements were taken on three separate days during 2003: 31 March, 14 May, and 22 May. Fracture density was measured using the circle-inventory approach of Davis and Reynolds (1996) and employing a 0.84-m-diameter hula hoop. A total fracture length was determined by summing all the fracture lengths within the circle. Fracture density is expressed as the total fracture length divided by the area of the circle. Mineral saturation and inverse mass-balance model calculations were conducted using PHREEQC (Parkhurst and Appelo, 1999).

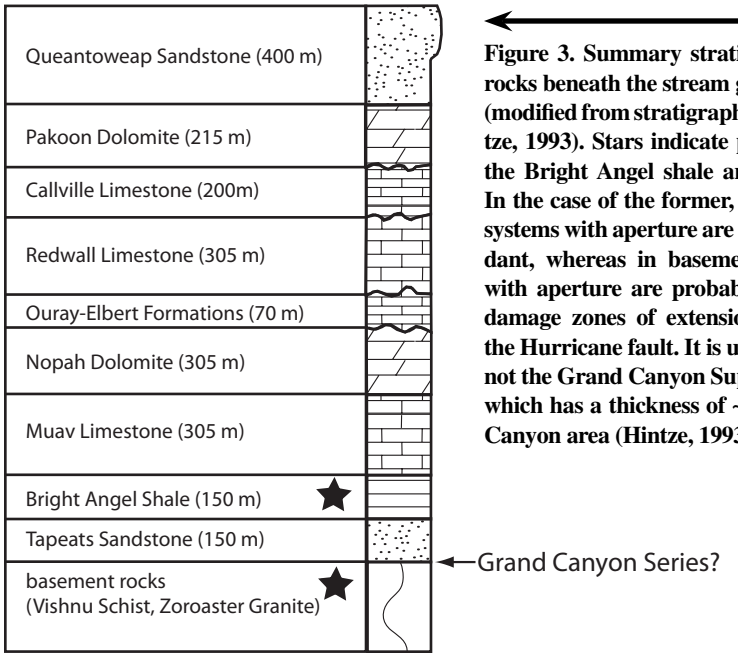

Figure 3. Summary stratigraphic section for rocks beneath the stream grade at Pah Tempe (modified from stratigraphic section 96 of Hintze, 1993). Stars indicate probable aquitards, the Bright Angel shale and basement rocks. In the case of the former, large-scale fracture systems with aperture are unlikely to be abundant, whereas in basement rocks, fractures with aperture are probably restricted to the damage zones of extensional structures like the Hurricane fault. It is unknown whether or not the Grand Canyon Supergroup is present, which has a thickness of ~4 km in the Grand Canyon area (Hintze, 1993).

TABLE 1. NEW CARBON AND HELIUM ISOTOPE DATA FOR PAH TEMPE GASES

Sample	$\delta^{13}C$ (CO_2) (‰)	$^3He/^4He$ (R/R_s)	^4He (cm^3 STP/cm^3 x 10^{-4})
21272	–5.3 (±0.2)	–	–
Pah Tempe 1.1	–5.7 (±0.2)	–	–
Virgin 4	–5.9 (±0.2)	–	–
Virgin 1	–	0.1072 (±0.003)	3.39 (±0.10)
Virgin 2	–	0.1023 (±0.001)	0.294 (±0.003)
Virgin 3	–	0.0977 (±0.001)	0.527 (±0.005)
Pah Tempe 1.2	–	0.0989 (±0.001)	2.13 (±0.064)

Data discussed in this paper are derived largely from Dutson (2005), which can be accessed online at http://etd.byu.edu/. However, data subsequently collected by us may be found in Table 1.

RESULTS

Water Composition

Water flowing in the Virgin River upstream of the springs is a dilute, mixed cation-anion water with an ionic strength of 0.012 mol/L. Spring discharge, by contrast, is Na^+-Cl^- water with appreciable Ca^{2+} and SO_4^{2-} (Fig. 2) and an ionic strength of ~0.2 mol/L. Although, in relative terms, carbonate species are not abundant, the calculated P_{CO_2} value of the water remains quite high ($\log P_{CO_2} \approx -0.18$) by the time it can be returned to the laboratory and analyzed. Spring water is oversaturated in quartz, aragonite, dolomite, and calcite, whereas it is undersaturated in gypsum and anhydrite. The high ionic strength of the springs so degrades water quality in the Virgin River (Fig. 2) that flows have been diverted around the spring discharges for agricultural and culinary uses for ~100 yr. At the time data were collected for this study, solute contents in the stream below Pah Tempe were dominated by an ~85% contribution of spring flux.

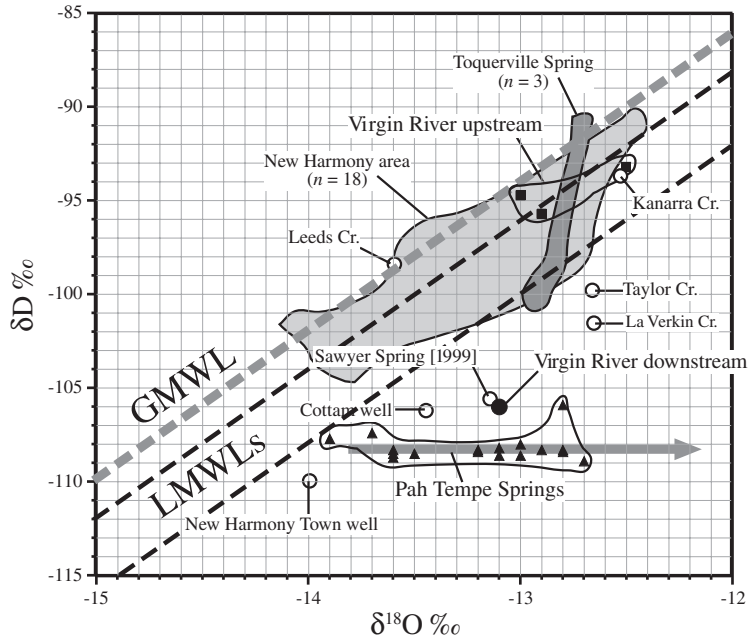

Figure 4. Oxygen and hydrogen isotope relationships of upstream water in the Virgin River, Pah Tempe spring discharge, and mixed downstream waters (Dutson, 2005) compared to other regional waters, including springs, wells, and creeks (A. Mayo, 2007, personal commun.). The point for 1999 Sawyer Spring may be an analytical outlier as it matches poorly with other analyses of this spring plotted within the New Harmony data field. The global meteoric water line (GMWL, $\delta D = 8\delta^{18}O + 10$; Craig, 1961) is shown for reference, as are bounding values for local meteoric water lines (LMWLs) based upon a map of the deuterium excess factor for January precipitation in southern Utah (IAEA, 2001).

Gas Flux

Gas-phase exsolution occurs as individual bubble trains arising through the stream, often occurring in groups or clusters. In total, more than an estimated 2400 individual bubble trains were found in the stream discharging a cumulative ~4–5 L/s. Because discrete spring discharges occur up to a few meters above stream level, invisible gas discharges almost certainly occur above stream level as well. The 10 vents for which flow rates were explicitly measured varied from 0.003 to 0.08 L/s.

On a blustery day in March 2007, when CO_2 outgassed from spring pools would be rapidly advected away, atmospheric concentrations varied from 560 ± 65 ppmv just above the surface of a well-exposed pool of spring water (developed for bathing), indicating that CO_2 is also lost directly from water surfaces. This represents an additional component of CO_2 loss that is difficult to quantify, but it indicates that estimates of CO_2 discharge represent minimum values.

Water and Gas Isotope Compositions

Stable isotope compositions of stream flows in the Virgin River above Pah Tempe plot on or below the global meteoric water line (GMWL, $\delta D = 8\delta^{18}O + 10$; Craig, 1961; Fig. 4), consistent with lower deuterium excess values of 4–8 as predicted by global precipitation maps for southern Utah (IAEA, 2001). Spring flows at Pah Tempe, by stark contrast, have nearly uniform δD values of about −108‰, whereas $\delta^{18}O$ values vary by >1‰ (Fig. 4). Spring waters plot in a horizontal linear trend well to the right of the meteoric water line.

Gas chromatographic analysis of exsolved gas flux detected essentially pure CO_2 (A. Mayo, 2007, personal commun.), although the odor of H_2S in the area is unmistakable. This gas has a $\delta^{13}C$ value of −5.3‰ to −5.9‰ (Table 1), compared to −2.1‰ for the DIC of spring water. The mean pH of the spring water is 6.3 ± 0.1, which is essentially the equivalence point for HCO_3^- and H_2CO_3 activities at the temperature of the springs, and it has an approximate P_{CO_2} value of 0.65 atm. HCO_3^- and H_2CO_3 are present in subequimolar proportions (~19 vs. ~14 mmol/kg, respectively), and the differences are due in part to the large difference in activity coefficients between charged and uncharged species in this brackish water. The weighted fractionation predicted by fractionation factors of Deines et al. (1974) between DIC species and CO_2 according to their relative abundances is ~3.6‰, which is

effectively equivalent to the observed difference of 3.2‰ to 3.8‰. Measured $^{3}He/^{4}He$ ratios from four vents exhibit a small range from 0.098 to 0.107 R_a (Table 1).

Water Flux

After subtracting the component of flow in the stream at the time of measurement (~40 L/s), spring discharge contributes ~260 L/s at Pah Tempe. When compared against gas vents, cumulative gas exsolution is well correlated with cumulative spring flows (Fig. 5), as expected. Based on vent counts, CO_2 release by gas bubble trains is ~5 L/s. As will be shown in the following sections, this is only a small fraction of total CO_2 released and carried downstream as the dissolved species HCO_3^- and H_2CO_3.

Fracture Density and Water-Flux Correlation

Fractures in Timpoweap Canyon have a general strike of north to N30°E, subparallel to the Hurricane fault (Fig. 6), 60% of the fractures are ≤1 mm in width, 35% are 2–5 mm in width, and 5% are >9 mm. Measured fracture densities in carbonate rock in the north wall of Timpoweap Canyon vary in a highly irregular fashion eastward of the fault (Fig. 7). The fracture density in the footwall of the easternmost major strand of the Hurricane fault (Fig. 1) correlates well with the density of bubble trains in the riverbed. We did not observe major discharges west of the fault. Although the discharge in the hanging wall of the fault has not been thoroughly evaluated, the highly impermeable nature of the poorly indurated siltstones and shales of the Moenkopi Formation makes flow of carbon dioxide unlikely through the hanging wall (Fig. 2).

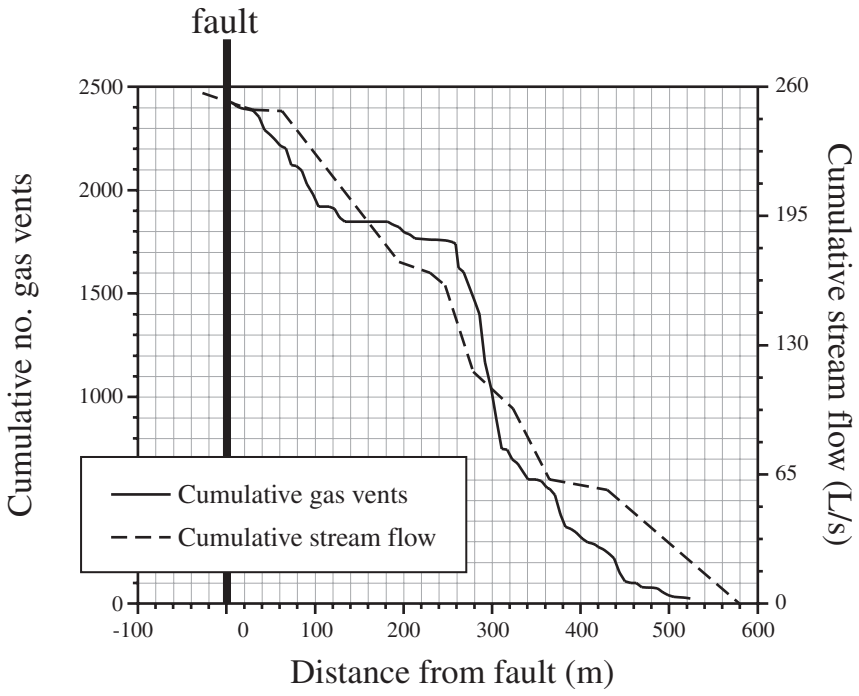

Figure 5. Relationship of cumulative gas vents counts to cumulative spring inflows in the Virgin River at Pah Tempe.

DISCUSSION

Source of Spring Waters

The residence time of the spring waters is difficult to determine directly. The spring discharges are tritium free, and our experience has shown that direct attempts to date these waters by ^{14}C methods would be unsuccessful due to elevated P_{CO_2} and accompanying enriched $\delta^{13}C$ values. Such waters have extraneous sources of carbon that are difficult to account for, making any realistic estimate of the proportion ^{14}C activity due to decay impossible.

As hydrothermal exchange (discussed later) likely produced little significant shift in hydrogen isotopes, it appears that the waters that fed this system, at the time of recharge, were isotopically depleted (with some exceptions) by as much as 18‰ relative to uplands contributing to modern recharge and surface flows in the Virgin River and other springs, wells, and surface waters in the region (Fig. 4). However, since the Virgin River drains much the same or similar recharge areas for springs of the region (Fig. 8), isotopic depletion at Pah Tempe may represent recharge under colder climate conditions. A maximum 18‰ difference in δD values corresponds only to an ~3 °C change in average temperature (Dansgaard, 1975), but it is difficult to envision a cause other than climate change for the depleted δD values of Pah Tempe springs relative to most waters in the area. Thus, these waters are likely to be at least as old as the end of the last glaciation (>10 ka), which is consistent with their deep circulation.

Pah Tempe spring discharge may include what has recently been referred to as "endogenic" water (e.g., Crossey et al., 2006; Liu et al., 2003), which is characterized by high P_{CO_2} values, elevated salinity, and low pH commonly associated with upwelling along faults. At Pah Tempe, the waters are conspicuously shifted to the right of both global and expected local meteoric water lines (Fig. 4), a phenomenon long associated with hydrothermal exchange of oxygen isotopes with crustal rocks at elevated temperatures of at least 100 °C or perhaps more (150–350 °C according to Criss [1999]). Dutson (2005) presented geothermometric calculations for these waters. Conductive and adiabatic thermometers produced estimated temperatures of ~70–75 °C, whereas silica thermometers (for quartz) produced maximum temperatures nearly equivalent to the discharge temperature. Clearly, these waters have been circulated slowly enough for them to cool to a temperature of ~40 °C, and they have largely reequilibrated in the process.

Although there is a record of ca. 350 ka basaltic volcanism in the immediate vicinity (Sanchez, 1995), it represents eruption from monogenetic cinder cones and associated lava flows fed from deep-crustal or upper-mantle magma chambers. Thus, we consider Quaternary volcanism an unlikely direct heat source for hydrothermal exchange, although magmatism may be related to a regionally elevated geotherm.

The mean annual air temperature in the area is ~16 °C. In order for water to have been heated more than 85–135 °C above mean annual air temperature (>100–150 °C by deep circulation), depths on the order of >3–5 km must have been achieved, assuming a relatively high geothermal gradient of 30 °C/km. A lower geotherm would require even deeper circulation. Dutson (2005) reported that there are ~2 km of Phanerozoic sedimentary cover above basement rock in the region; thus, these waters have almost certainly circulated through crystalline basement rock. For example, most of Hintze's (1993) stratigraphic sections for southwestern Utah lack Neoproterozoic sedimentary rocks that occur

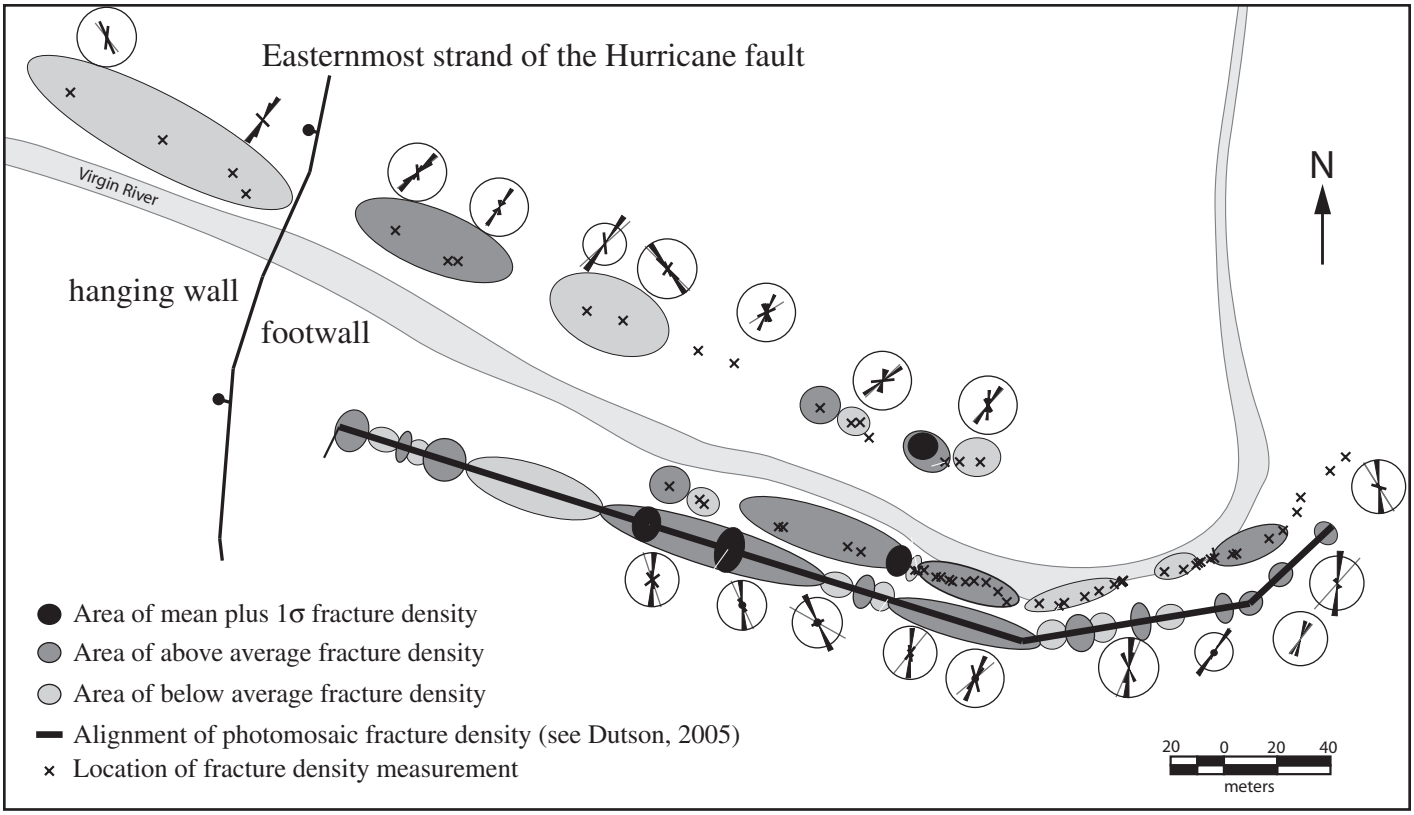

Figure 6. Map of fracture orientations and fracture densities within Timpoweap Canyon. Note that major fracture sets tend to be subparallel to the Hurricane fault, which is a tectonically active structure. A summary of photomosaic fracture mapping is also reported (see Dutson, 2005, for details).

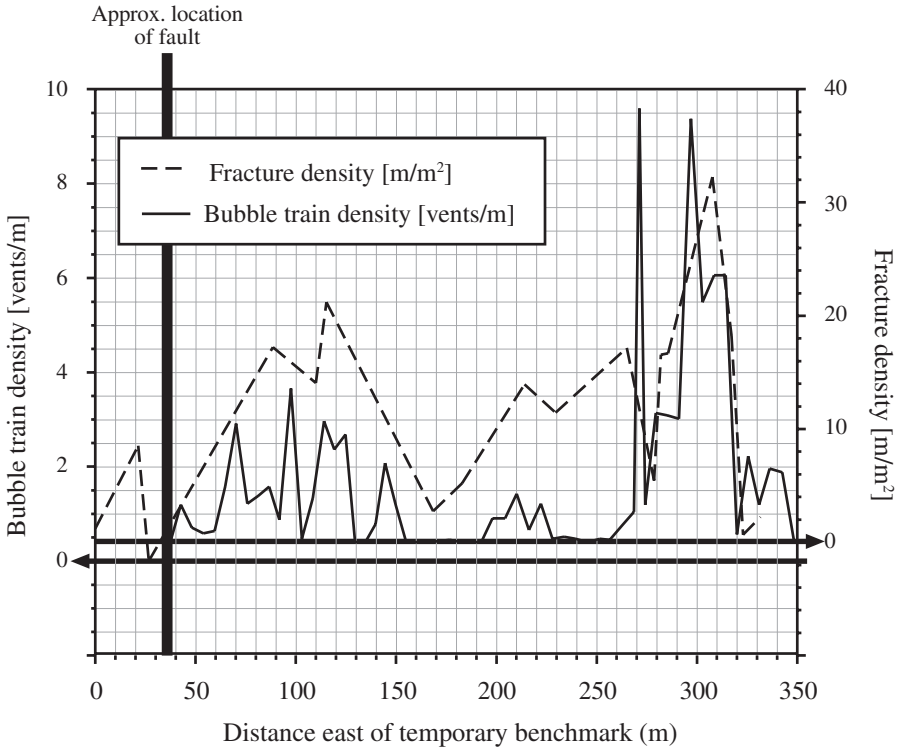

Figure 7. East-west projection of the relationship of fracture density (m/m²) in carbonate rocks above the streambed to gas vent counts within the stream. Note that because the fracture measurements were taken in the north canyon wall, rather than within the stream itself, the projection produces some uncertainty in the match of the two features.

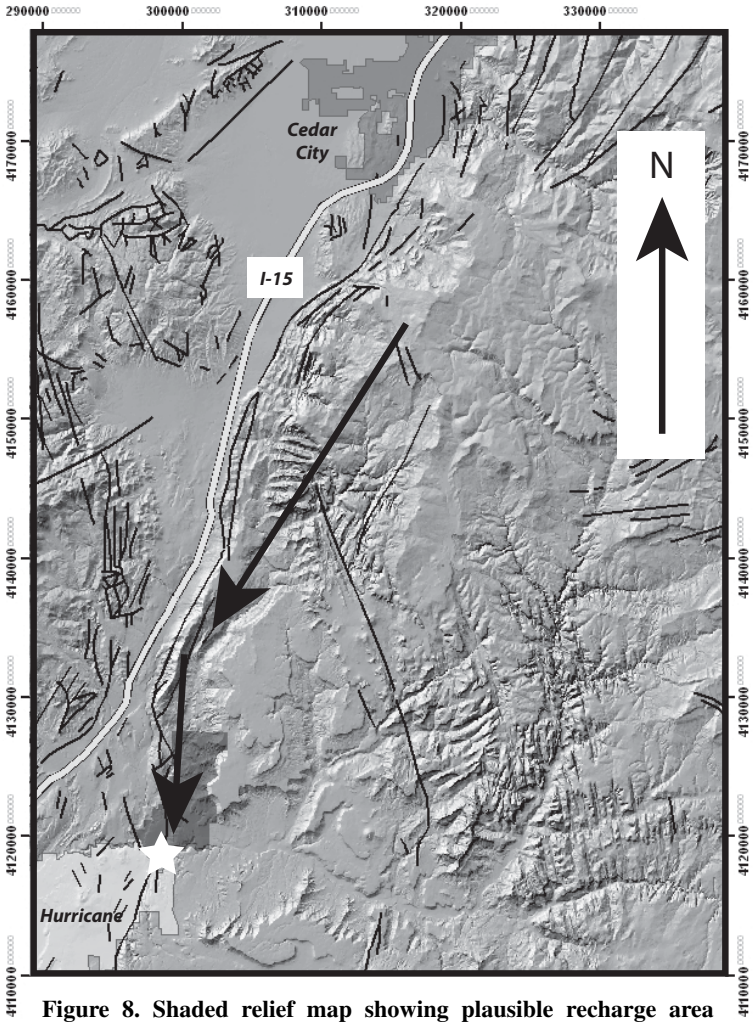

Figure 8. Shaded relief map showing plausible recharge area and flow paths for waters discharging at Pah Tempe. Faults were derived from Hintze et al. (2000). Map projection is in universal transverse Mercator (UTM) coordinates, zone 12N.

elsewhere in the Colorado Plateau. However, without drilling data, we cannot determine for certain whether or not they are present beneath Pah Tempe. Assuming they are absent, such high fluxes through crystalline basement rock were probably facilitated by open fractures produced by slip on the Hurricane fault in an extensional stress regime and augmented by high fluid pressure at depth. If these rocks are present, they could be sufficiently thick (~4 km) to preclude flow through basement.

Water-Rock Interactions

The hydrothermal shift in $\delta^{18}O$ values could provide important information on the temperature of exchange, and therefore depth of circulation, if the lithology and mechanism of isotope exchange were known. For example, Valley (2001) calculated closure temperatures (after Dodson, 1973) to the self-diffusion of oxygen in important rock-forming minerals, including feldspar, quartz, and calcite. In most cases, it appears that oxygen isotope enrichment of water by self-diffusion takes place at temperatures in excess of 300 °C, corresponding to mid-crustal levels.

We have independently verified the conclusions of Valley (2001) in Table 2A, even for very fine grains of quartz and calcite (0.01 cm radius). Feldspar, however, could undergo diffusive exchange at temperatures as low as 150 °C, although this analysis reveals nothing regarding how rapidly this exchange could proceed. Clay minerals, by contrast, are capable in principle of exchange at near-surface conditions, but if this exchange were rapid on geological time scales, we would expect to observe oxygen isotope enrichment much more frequently.

In the event of recrystallization, however, apparent closure temperatures for rocks and minerals are similar to near-surface values (Table 2B). These dynamic processes are capable of modifying the isotopic composition of aqueous fluids, but if they are important, it begs the question as to why most waters lack obvious evidence of exchange at low temperature.

A consideration of the mechanisms of water-rock exchange of oxygen, in the end, is impossible because we have no direct evidence of the mechanism (self-diffusion versus chemical reaction) involved. Thus, we agree with conventional wisdom suggesting that moderately high temperatures (>150 °C) and circulation depths (>5 km) were achieved, and that this likely involved flow through the basement (Fig. 3).

Correlation of Discharge to Fractures

The correlation of gas and water inflow from an aquifer to observable fracture density above the aquifer (Fig. 6) suggests that secondary subsurface fracture permeability is providing the pathways for fluid flow to the surface. In Timpoweap Canyon, clusters of high fracture density are clearly associated with gas vents, and because gas vents are correlated to spring inflows, groundwater discharge is also related to clusters of high fracture density (Fig. 6). Large-scale faults are commonly surrounded by clusters of smaller-scale fractures and faults in the fault-damage zone. Transects of structural frequency across fault-damage zones usually show a significant degree of clustering of minor faults and fractures and may show an overall increase toward the major slip plane (see review in Odling et al., 2004).

As noted already, the measured fractures mostly trend subparallel to the NE trend of the Hurricane fault (Fig. 6) and dip subvertically. Fractures of this trend are likely to maintain some aperture as they are subparallel to an active extensional fault. Assuming that fractures within the Seligman Member have aperture distributions similar to those described previously, and because flux within a fracture scales with the cube of aperture (Bear, 1972), >70% of the discharge could be partitioned into the 5% of fractures with >9 mm width. The localization of flow through a small number of fractures is not unusual in fracture-dominated flow. For instance, Evans et al. (2005) showed that just 10 major open fractures within a single fault zone located at 3490 m depth accounted for 95% of the flow into boreholes at the European Union's Soultz-sous-Forêt Hot Dry Rock test site.

Although the distribution of fracture apertures within the subjacent Queantoweap Sandstones and Seligman Member is unknown, it is a relatively simple matter to demonstrate that relatively few fractures are needed to sustain the

TABLE 2A. CLOSURE TEMPERATURES (°C) CALCULATED AFTER DODSON (1973) BASED ON EXPERIMENTAL DATA COMPILED IN COLE AND CHAKRABORTY (2001)

Mineral	Grain radius 0.01 (cm)	Grain radius 0.1 (cm)	Grain radius 1 (cm)	Reference*
Anorthite	167	241	343	Giletti et al. (1978)
Albite	143	227	350	Giletti et al. (1978)
Calcite	307	386	491	Farver (1994)
Quartz	493	676	964	Dennis (1984a)
Quartz	510	616	754	Giletti and Yund (1984)
Quartz	481	596	750	Giletti and Yund (1984)
Kaolinite	<54			O'Neil and Kharaka (1976)
Kaolinite	<49			O'Neil and Kharaka (1976)
Kaolinite	<103			Lui and Epstein (1984)
Illite	<0			O'Neil and Kharaka (1976)
Illite	<0			O'Neil and Kharaka (1976)

Note: Experiments were chosen in the presence of 100 MPa water (±solutes) and interpreted to result from self-diffusion rather than chemical reaction. A 5 °C/m.y. cooling rate was employed based upon the Hurricane fault slip rate of ~0.2 mm/yr at Pah Tempe (Lund et al., 2002) and an assumed geothermal gradient of 25–30 °C. A spherical shape factor was used in all cases.

*Complete documentation and references for the data sources, experimental conditions, etc., are provided in Cole and Chakraborty (2001).

TABLE 2B. CLOSURE TEMPERATURES (°C) CA LCULATED AFTER DODSON (1973) BASED ON EXPERIMENTAL DATA COMPILED IN COLE AND CHAKRABORTY (2001)

Mineral	Grain radius 0.01 (cm)	Grain radius 0.1 (cm)	Grain radius 1 (cm)	Reference*
Granite			<0	Cole et al. (1992)
Basalt			<0	Cole et al. (1992)
Albite	<0	14	45	O'Neil and Taylor (1967)
Microcline			<0	Cole et al. (1992)
Sanidine			<0	O'Neil and Taylor (1967)
Calcite			<0	O'Neil et al. (1969)

Note: Experiments were interpreted to result from "chemical reaction" (recrystallization or cation exchange) rather than self-diffusion. A 5 °C/m.y. cooling rate was employed based upon the Hurricane fault slip rate of ~0.2 mm/yr at Pah Tempe (Lund et al., 2002) and an assumed geothermal gradient of 25–30°C. A spherical shape factor was used in all cases.

*Complete documentation and references for the data sources, experimental conditions, etc., are provided in Cole and Chakraborty (2001).

observed flow in either unit. Equation 1 is the familiar cubic law for flux (Q per unit length of fracture), where

$$Q = \frac{b^3}{12\mu}\rho g, \quad (1)$$

μ and ρ are the dynamic viscosity and density of water (6.53×10^{-4} kg/m s, and 992.25 kg/m^3 at 40 °C), and b is fracture aperture. The stream is ~30 m wide (i.e., 30 unit lengths) near the bend of the river (Fig. 2), and on the south side of the stream there are large discharges from fractures in the canyon wall into developed bathing pools that occur 2–3 m above stream level.

This formulation of the cubic law, which does not account for fracture roughness or variable aperture, can account for the observed flux with <10 fractures of 30 m length and just 1 mm aperture. This clearly indicates that neither fracture nor matrix permeability in the Queantoweap Sandstone is a limiting factor on discharge.

The correlation of gas and water discharge to fracture density in the canyon walls indicates that the Hurricane fault damage zone in the low-permeability gypsiferous siltstone of the Seligman Member of the Kaibab Formation provides a pathway for flow out of the Queantoweap Sandstone. Although the sedimentology of the Queantoweap Sandstone is variable, it is dominated by eolian facies, which are likely to have high primary porosity and permeability. Butler (1995) reported that the Queantoweap Sandstone has produced good hydrocarbon shows, so at least in places, this unit is a regional flow unit. The damage zone in high-porosity sandstones will be dominated by relatively low-porosity deformation bands and high-permeability slip surfaces, but it is probable that the fault-damage zone in the Queantoweap contributes to impeding across-fault flow but does not provide a barrier to flow up the fault (Shipton et al., 2002, 2005b; Fossen et al., 2007).

Source of CO_2 and its Flux

Exsolved gas from the springs at Pah Tempe consists of nearly pure CO_2. Natural CO_2 in such high concentrations can only originate from two sources, namely mantle volatile degassing or thermal metamorphism of carbonates. The measured range of $\delta^{13}C$ (CO_2) values from −5.3‰ to −5.9‰ (Table 1) is within the cited range of mantle-derived carbon of −3‰ to −8‰. However, this range overlaps with that of bulk crustal carbon, −5‰ to −7‰, and therefore does not provide unequivocal evidence of a mantle or crustal origin for the CO_2 emanating from the springs (Ballentine, 1997; Ballentine et al., 2001, 2002; Coltice et al., 2004; Javoy et al., 1986; Jenden et al., 1993; Lollar et al., 1997).

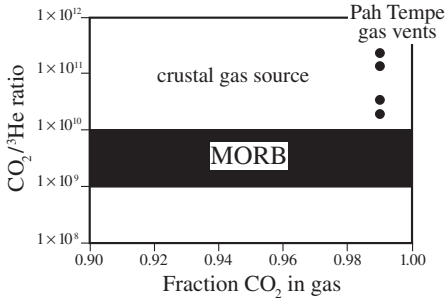

Figure 9. All of the Pah Tempe springs exsolve gas that has a $CO_2/^3He$ ratio above the mid-ocean-ridge basalt (MORB) range, indicating that the CO_2 is predominantly derived from a crustal source (Sherwood Lollar et al., 1997; Ballentine et al., 2001, 2002; Zhou et al., 2005). All error bars are smaller than printed symbols. The shaded region highlights the range of $CO_2/^3He$ values measured in pure magmatic samples (MORB) (Burnard et al., 1997, 2002; Moreira et al., 1998).

Noble gases, specifically ^3He, are unambiguous tracers of the mantle volatile contribution to a crustal fluid because ^3He is primordial in origin and is not produced in significant quantities within the crust. Figure 9 shows measured $CO_2/^3He$ ratios plotted against CO_2 composition for four of the Pah Tempe CO_2 gas samples. All of the samples have $CO_2/^3He$ ratios above the mid-ocean-ridge basalt (MORB) range of 1×10^9 to 1×10^{10}. Hence, it can be concluded that the CO_2 sampled at the surface is predominantly derived from the thermal metamorphism of carbonates. However, it is impossible to determine if this crustal $CO_2/^3He$ signature is the result of the addition of crustal CO_2 free from ^3He on migration to the surface or if it represents the original source $CO_2/^3He$ ratio of the CO_2 prior to migration.

Measured $^3He/^4He$ ratios exhibit a small range from 0.098 to 0.107 R_a (Table 1), which is slightly above the crustal $^3He/^4He$ R_a value of 0.02 and significantly below the measured subcontinental mantle ratio of the region of 4.5–7.7 R_a (Fitton et al., 1991; Dodson et al., 1998; Reid and Graham, 1996). This implies that there is a small mantle contribution to the CO_2. This range of ratios is also significantly below that of air, and, combined with the high He concentrations (which range from 5.7 to 65 times greater than

air), it allow us to rule out atmospheric contamination of the samples.

The proportion of ^{3}He and ^{4}He from the mantle and crust can be calculated using the crust end-member value and an averaged subcontinental mantle ^{3}He/^{4}He value of 6 R_a (Eq. 2),

$$^4\mathrm{He}_{\mathrm{crust}} = \frac{\frac{^3\mathrm{He}}{^4\mathrm{He}_{\mathrm{mantle}}} - \frac{^3\mathrm{He}}{^4\mathrm{He}_{\mathrm{measured}}}}{\frac{^3\mathrm{He}}{^4\mathrm{He}_{\mathrm{mantle}}} - \frac{^3\mathrm{He}}{^4\mathrm{He}_{\mathrm{crust}}}}, \quad (2)$$

where $^4\mathrm{He}_{\mathrm{crust}}$ denotes the proportion of crustal ^{4}He within a unit volume of gas.

The crustal contribution to ^{4}He is extremely high, ranging from 98.54% to 98.70%, with the remainder originating from the mantle. The crustal contribution to ^{3}He can also be calculated using the following formula:

$$^3\mathrm{He}_{\mathrm{crust}} = \left({}^3\mathrm{He}_{\mathrm{crust}} \times \frac{^3\mathrm{He}}{^4\mathrm{He}_{\mathrm{crust}}} \right) \div \left[\left({}^3\mathrm{He}_{\mathrm{crust}} \times \frac{^3\mathrm{He}}{^4\mathrm{He}_{\mathrm{crust}}} \right) + \left(1 - {}^4\mathrm{He}_{\mathrm{crust}} \times \frac{^3\mathrm{He}}{^4\mathrm{He}_{\mathrm{mantle}}} \right) \right]. \quad (3)$$

Despite virtually all of the ^{4}He originating from the crust, only 18.4%–20.2% of the total ^{3}He can be attributed to the crust, with the remainder originating from the mantle. These figures can be used with the range in mantle $CO_2/^3$He ratios of 1×10^9 to 1×10^{10} to calculate the contribution of CO_2 from the mantle and crust, ignoring the atmosphere contribution for the reasons outlined already. An unknown factor is the crustal $CO_2/^3$He ratio, which is variable (e.g., O'Nions and Oxburgh, 1988). However, a simple mass-balance approach allows the crustal $CO_2/^3$He ratio range to be calculated, from which both the crust and mantle contributions follow. We assume that gases other than CO_2 have negligible overall volume.

$$\left({}^3\mathrm{He}_{\mathrm{mantle}} \times \frac{\mathrm{CO}_2}{^3\mathrm{He}_{\mathrm{mantle}}} \right) + \left({}^3\mathrm{He}_{\mathrm{crust}} \times \frac{\mathrm{CO}_2}{^3\mathrm{He}_{\mathrm{crust}}} + \mathrm{CO}_{2,\mathrm{air}} \right) = 1. \quad (4)$$

The results of the calculation are shown in Table 3. As expected, the crustal contribution to the CO_2 is high, ranging from a minimum of 58.5% (Virgin 1) to 96.6% (Virgin 2) using a $CO_2/^3\mathrm{He}_{\mathrm{mantle}}$ value of 1×10^{10}. The maximum crustal contribution using a $CO_2/^3\mathrm{He}_{\mathrm{mantle}}$ ratio of 1×10^9 is 95.9% (Virgin 1) to 99.7% (Virgin 2). The calculated $CO_2/^3$He ratios for the crust vary from 6.3×10^{10} to 1.2×10^{12}, which are within the range considered by O'Nions and Oxburgh (1988) to be typical of the crust.

TABLE 3. ESTIMATES OF CRUST AND MANT LE GAS CONTRIBUTIONS AT PAH TEMPE

Sample	Using $CO_2/^3\mathrm{He}_{\mathrm{mantle}}$ of 1×10^9			Using $CO_2/^3\mathrm{He}_{\mathrm{mantle}}$ of 1×10^{10}		
	CO_2 origin %		Crust $CO_2/^3$He	CO_2 origin %		Crust $CO_2/^3$He
	Crust	Mantle		Crust	Mantle	
Virgin 1	95.85	4.15	1.03×10^{11}	58.50	41.50	6.26×10^{10}
Virgin 2	99.66	0.34	1.23×10^{12}	96.60	3.40	1.19×10^{12}
Virgin 3	99.43	0.57	6.83×10^{11}	94.25	5.75	6.48×10^{11}
Pah Tempe 1.2	97.64	2.36	1.66×10^{11}	76.42	23.58	1.30×10^{11}

Unfortunately, it is not possible to determine whether all the crustal CO_2 component is derived from deep crustal decarbonation reactions versus the contribution from aquifer water that has dissolved carbonate minerals. The regional stratigraphy includes a considerable volume of marine carbonate rocks beneath the structural level of the springs. However, the high DIC content suggests that an upward flux of CO_2 within the fault zone would be required to provide sufficient acidity and accompanying carbonate dissolution to accommodate the elevated HCO_3^- and H_2CO_3 activities.

A simple calculation comparing the flux of exsolved to dissolved CO_2 due to spring discharge shows that the gas phase only represents ~2% of the total (Table 4) carbon flux. Thus, a quantitative treatment of CO_2 loss through the enhanced permeability in the footwall of the Hurricane fault must focus on the dissolved species.

This observation can account for the variation in He concentrations within the samples. As the gas phase only represents 2% of the CO_2 flux erupting from the springs, it is highly probable that all of the CO_2 is traveling to the surface dissolved in the groundwater. As there is therefore no free-gas phase, all of the ^{3}He transported to the surface will also be dissolved in the groundwater. When reaching the surface, 2% of the CO_2 is exsolved as gas, and because He is extremely insoluble, all of the dissolved ^{3}He will exsolve into this CO_2 gas phase. While the gas phase sampled contains almost pure CO_2, variable amounts will have been degassed at the different sample localities, and hence variable dilution of the ^{3}He will have occurred. Since this is the case, our calculations of the proportion of crustal CO_2 within the springs should be taken as a minimum, as exsolution of more CO_2 would further dilute the ^{3}He concentrations and increase the overall $CO_2/^3$He ratios.

Some of the DIC at Pah Tempe was obtained in the soil zone during recharge. We attempted to constrain an upper limit to the DIC content of recharge in order to estimate the minimum flux of CO_2 from the system that has been added in the subsurface. Using the average winter solute content of meteoric water from a nearby NADP site (National Atmospheric Deposition program), we employed a simple PHREEQC (Parkhurst and Appelo, 1999) calculation. In order to obtain charge balance, the reported Na^+ content was increased from 0.08 to 0.16 mg/L. Precipitation was allowed to come into equilibrium with calcite at an elevated soil $P_{CO_2} = 10^{-2}$, simulating maximum acidification of groundwater by soil-zone CO_2 that was then expended dissolving calcite during recharge. At the resulting pH (~7.3), a maximum of about ~4.2 mmol/kg out of a total of ~34.6 mmol/kg could be derived from recharge. However, the remaining ~30.2 mmol/kg of the DIC load is likely to be extraneous, derived from an upwelling gas flux within the footwall damage zone, perhaps accompanied by additional dissolution of carbonate minerals.

PHREEQC inverse mass-balance models were employed to more explicitly estimate the fraction of CO_2 gas dissolved in the spring water relative to carbonate dissolution during chemical evolution from recharge to discharge compositions. Besides the inclusion of obvious phases (calcite, dolomite, gypsum, halite, and CO_2), mass balances were achieved by the inclusion of ion exchange for K^+, Na^+, Ca^{2+}, and Mg^{2+}. Although these constraints readily produced model solutions, these solutions violated solubility constraints. For example, many models

TABLE 4. COMPARISON OF THE ESTIMATED AND POTENTIAL CO_2 FLUXES AT PAH TEMPE

Annual evolved CO_2 flux (mol/yr)	Gross annual dissolved CO_2 flux (mol/yr)	Net annual dissolved CO_2 flux (mol/yr)
6.1×10^6	2.8×10^8	2.5×10^8
Hypothetical CO_2 flux (mol/yr) at 30 MPa and 50–150 °C		
2.0×10^9 to 4.1×10^9		

required the dissolution of dolomite, whereas Pah Tempe spring water is oversaturated in this phase. Three realistic models consistent with solubility relations were produced by the inclusion of Mg-alumino-silicates such as talc and sepiolite to approximate interaction with Mg-clays.

These three models infer the dissolution of 3.0×10^{-2} to 3.5×10^{-2} mol/kg of dissolved CO_2. At the lower end of this range, a CO_2 flux of 2.5×10^8 mol/yr can be derived, which is the same value as our estimated net annual flux (Table 4) after accounting for DIC loads added during recharge. Thus, it appears that the majority of carbon exiting the subsurface at Pah Tempe is the result of the quantitative dissolution of CO_2 in the subsurface prior to discharge.

Size of the CO_2 Source

An important question is whether the release of CO_2 is limited by the size of the reservoir, or if it is limited by the ability of water to leave the subsurface. As discussed here, water flux seems to be limited by the permeability of the Seligman Member. The total carbon content of Pah Tempe spring discharge is ~3.5×10^{-2} mol/kg. For example, at an assumed circulation depth of 3 km, or a hydrostatic pressure of ~30 MPa, the solubility of CO_2 in pure water is much higher (~0.25–0.50 mol/kg) over a temperature range of 50–150 °C (Fig. 4 of Portier and Rochelle, 2005). At the salinity of Pah Tempe water, this solubility is reduced slightly to ~95% of this value (Kansas Geological Survey, 2003), or ~0.24–0.48 mol/kg. Although many other factors, such as pH, may influence the solubility of CO_2, this calculation infers that the rate of CO_2 production and transport to the aquifer is much lower than the ability of the aquifer to deliver CO_2 to the surface.

Small volumes of tufa are currently being deposited at a few discrete discharge locations along the banks of the Virgin River just above stream level. However, most discharge is directly into the streambed. Fracture-filling calcite veins are also observed near sites of current discharge within the carbonate rocks that form the cliffs, as well as remnants of tufa preserved on at least the lower portions of the canyon walls.

Careful U-series analysis of these vein carbonates could be employed to constrain the minimum length of time that CO_2 loss has proceeded, but it represents a substantial undertaking that remains to be done. Lund et al. (2002) estimated current slip rates on the Hurricane fault to vary from 0.21 to 0.57 mm/yr. Assuming that these figures bracket the long-term slip history of the fault, and that development of the Hurricane fault initiated outgassing at Pah Tempe, its history could easily extend back well into the Miocene Epoch in order to accommodate the 2370 m of throw on the fault at this location, and far beyond the utility of the U-series geochronometers. However, this maximum age is quite speculative.

What is also unknown is whether or not the fracture permeability in the fault zone is self-sealing. As noted herein, these spring waters are oversaturated in carbonate minerals, so there may be a natural tendency for deposition to diminish fracture permeability over time, an observation that is consistent with calcite-filled fractures. If the repose interval between large subsequent earthquakes (several k.y. to more than 10 k.y.; Lund et al., 2002) is large relative to the time scale for fracture sealing, spring discharge may represent transient events following large earthquakes.

A slip event (>M 5.8) that occurred in 1992 along the Anderson Junction segment of the Hurricane fault included the Pah Tempe area and altered spring flows (Blackett, 2004). Additional evidence that slip events may affect discharge derives from blasting in 1985 near the springs, which also altered flows and discharge locations (Frandsen, 2004).

CONCLUSIONS

The thermal springs at Pah Tempe are a clear example of the discharge of CO_2 by deeply circulated upwelling fluids within the footwall damage zone of an active fault. Fracture systems in the walls of Timpoweap Canyon correlate well with water and gas discharge patterns. Thus, fracture mapping above the confining unit for the system reveals fundamental information regarding fracture permeability within or below the confining unit. Comparisons of fracture density and CO_2 flux show that as much as >70% of the flow may be focused in as little as 5% of the fractures. Although there is unlikely to be a large pool of supercritical CO_2 at depth below the Pah Tempe hot springs (the Queantoweap is too shallow and the volumes of CO_2 are not inferred to be large), it is essential to understand the controls on the generation of fracture clusters to be able to predict likely flow in future engineered storage sites, such as may be the case in geologic CO_2 sequestration.

Waters at Pah Tempe have been deeply circulated (>3–5 km?). This seemingly requires flow through crystalline basement rocks, resulting in water-rock exchange of oxygen isotopes. However, unless the mechanism and minerals involved in exchange are known, it is difficult to place further limits on temperatures and depths of circulation. Hydrogen isotopes suggest that these waters were recharged under colder climate conditions, consistent with long circulation time scales.

Pah Tempe illustrates that in many cases, a large majority of CO_2 may be returned to the surface within the DIC load. Geochemical models suggest that the DIC load is dominated by quantitative dissolution of gas rather than gas dissolution accompanied by carbonate mineral dissolution. Because most water at Pah Tempe discharges near or within the Virgin River itself, spring water is rapidly carried away, providing little opportunity for the development of extensive spring tufas. Thus, calcite volumes in tufa deposits cannot be used to estimate past fluxes under such circumstances.

The size of the CO_2 reservoir or gas production rate at depth appears to be small relative to the capacity of water to carry it to the surface. Noble gas analysis reveals the gas to be mostly crustal in origin. Calcite-filled veins and minor tufa remnants on cliff walls above stream level suggest that discharge has extended for a considerable period of time. Speculatively, the age of the Hurricane fault suggests outgassing could extend back into the Miocene Epoch.

The net flux rate of CO_2 at Pah Tempe is on the order of hundreds of millions of moles of carbon per year. As large as that may seem, it may be valuable to put the magnitude of this flux in perspective. It is a simple matter to demonstrate that the total contemporary CO_2 flux at Pah Tempe is only a very small fraction (<1%) of the gas released by a large (1000 MW) coal-fired power plant, and only several percent of the total, assuming CO_2 saturation at minimum circulation depths of ~3 km were reached. The current rate of natural release at a system like Pah Tempe is trivial compared to anthropogenic contributions.

ACKNOWLEDGMENTS

This work was supported by funds provided by the Brigham Young University College of Physical and Mathematical Sciences. Kip Solomon (University of Utah) and Tony Fallick (Scottish Universities Environmental Research Centre, East Kilbride) assisted with gas sample analysis. Constructive and thorough reviews were provided by Mark Person and three anonymous referees. Jerry Fairley assisted with formulation of the cubic law. Ken Anderson, owner of the Pah Tempe resort, is especially thanked for his cooperation and access over the last several years.

REFERENCES CITED

Ballentine, C.J., 1997, Resolving the mantle He/Ne and crustal $^{21}Ne/^{22}Ne$ in well gases: Earth and Planetary Science Letters, v. 152, p. 233–250, doi: 10.1016/S0012-821X(97)00142-8.

Ballentine, C.J., Schoell, M., Coleman, D., and Cain, B.A., 2001, 300-Myr-old magmatic CO_2 in natural gas reservoirs of the West Texas Permian Basin: Nature, v. 409, p. 327–331, doi: 10.1038/35053046.

Ballentine, C.J., Burgess, R., and Marty, B., 2002, Tracing fluid origin, transport and interaction in the crust: Noble gases in geochemistry and cosmochemistry: Reviews in Mineralogy and Geochemistry, v. 47, p. 539–614.

Bear, J., 1972, Dynamics of Fluids in Porous Media: New York, Dover, 784 p.

Benson, S.M., and Hepple, R., 2005, Prospects for early detection and options for remediation of leakage from CO_2

storage projects, *in* Thomas, D., and Benson, S.M., eds., Carbon Dioxide Capture for Storage in Deep Geologic Formations—Results from the CO_2 Capture Project, Volume 2: London, Elsevier Science, p. 1189–1203.

Biek, R., 2003, Geologic Map of the Hurricane Quadrangle Washington County, Utah: Utah Geological Survey Map 187, scale 1:24,000.

Blackett, R., 2004, St. George basin geothermal area: Geo-Heat Center Quarterly Bulletin, v. 25, p. 52–53.

Burnard, P., Graham, D., and Turner, G., 1997, Vesicle-specific noble gas analyses of "popping rock"; implications for primordial noble gases in Earth: Science, v. 276, p. 568–571, doi: 10.1126/science.276.5312.568.

Burnard, P.G., Graham, D.W., and Farley, K.A., 2002, Mechanisms of magmatic gas loss along the Southeast Indian Ridge and the Amsterdam–St. Paul Plateau: Earth and Planetary Science Letters, v. 203, p. 131–148, doi: 10.1016/S0012-821X(02)00828-2.

Butler, W.C., 1995, Northern Arizona Province (024), *in* Gautier, D.L., Dolton, G.L., Takahashi, K.I., and Varnes, K.L., eds., 1995, National assessment of United States Oil And Gas Resources—Results, Methodology, and Supporting Data: U.S. Geological Survey Digital Data Series DDS-30, Release 2, one CD-ROM: http://certmapper.cr.usgs.gov/data/noga95/prov24/text/prov24.pdf (2007).

Cole, D.R., and Chakraborty, S., 2001, Rates and mechanisms of isotopic exchange: Stable isotope geochemistry: Reviews in Mineralogy and Geochemistry, v. 43, p. 83–223, doi: 10.2138/gsrmg.43.1.83.

Coltice, N., Simon, L., and Lecuyer, C., 2004, Carbon isotope cycle and mantle structure: Geophysical Research Letters, v. 31, L05603, doi: 10.1029/2003GL018873.

Coplen, T.B., 1988, Normalization of oxygen and hydrogen isotope data: Chemical Geology, v. 72, p. 293–297.

Craig, H., 1961, Isotopic variations in meteoric waters: Science, v. 133, p. 1702–1703, doi: 10.1126/science.133.3465.1702.

Criss, R.E., 1999, Principles of Stable Isotope Distribution: Oxford, Oxford University Press, 254 p.

Crossey, L.J., Fischer, T.P., Patchett, P.J., Karlstrom, K.E., Hilton, D.R., Newell, D.L., Huntoon, P., Reynolds, A.C., and de Leeuw, G.A.M., 2006, Dissected hydrologic system at the Grand Canyon: Interaction between deeply derived fluids and plateau aquifer waters in modern springs and travertine: Geology, v. 34, p. 25–28, doi: 10.1130/G22057.1.

Dansgaard, W., 1975, Stable isotopes in precipitation, *in* Kitano, Y., ed., Geochemistry of Water: Stroudsburg, Pennsylvania, Dowden, Hutchinson & Ross, 455 p.

Davis, G., and Reynolds, S., 1996, Structural Geology of Rocks and Regions: New York, John Wiley, 776 p.

Deines, P., Langmuir, D., and Harmon, R.S., 1974, Stable carbon isotope ratios and the existence of a gas phase in the evolution of carbonate ground waters: Geochimica et Cosmochimica Acta, v. 38, p. 1147–1164, doi: 10.1016/0016-7037(74)90010-6.

Dodson, A., DePaolo, D.J., and Kennedy, B.M., 1998, Helium isotopes in lithospheric mantle; evidence from Tertiary basalts of the Western USA: Geochimica et Cosmochimica Acta, v. 62, p. 3775–3787, doi: 10.1016/S0016-7037(98)00267-1.

Dodson, M.H., 1973, Closure temperature in cooling geochronological and petrological systems: Contributions to Mineralogy and Petrology, v. 40, p. 259–274, doi: 10.1007/BF00373790.

Drimmie, R.J., Heemskerk, A.R., and Johnson, J.C., 1993, Tritium Analysis. Technical Procedure 1.0, Rev. 03: Waterloo, Ontario, Canada, Environmental Isotope Laboratory, Department of Earth Science, University of Waterloo, 27 p.

Dutson, S.J., 2005, Effects of Hurricane Fault Architecture on Groundwater Flow in the Timpoweap Canyon of Southwestern, Utah [M.S. thesis]: Provo, Brigham Young University, 57 p.

Epstein, S., and Mayeda, T., 1953, Variation of ^{18}O content of waters from natural sources: Geochimica et Cosmochimica Acta, v. 4, p. 213–224, doi: 10.1016/0016-7037(53)90051-9.

Evans, K.F., Genter, A., and Sausse, J., 2005, Permeability creation and damage due to massive fluid injections into granite at 3.5 km at Soultz: 1. Borehole observations: Journal of Geophysical Research, v. 110, doi: 10.1029/2004JB003168.

Fitton, J.G., James, D., and Leeman, W.P., 1991, Basic magmatism associated with late Cenozoic extension in the Western United States; compositional variations in space and time; Mid-Tertiary Cordilleran magmatism; plate convergence versus intraplate processes: Journal of Geophysical Research, v. 96, p. 13,693–13,711, doi: 10.1029/91JB00372.

Fossen, H., Schultz, R.A., Shipton, Z.K., and Mair, K., 2007, Deformation bands in sandstone—A review: Journal of the Geological Society of London, v. 164, p. 755–769, doi: 10.1144/0016-76492006-036.

Frandsen, N., 2004, Pah Tempe: Hurricane Valley Journal, v. 8, http://www.hvjournal.com/articles.php?is=1525 (2007).

Gehre, M., Hoefling, R., and Kowski, P., 1996, Sample preparation device for quantitative hydrogen isotope analysis using chromium metal: Analytical Chemistry, v. 68, p. 4414–4417, doi: 10.1021/ac9606766.

Hendry, M.J., Kotzer, T.G., and Solomon, D.K., 2005, Sources of radiogenic helium in a clay till aquitard and its use to evaluate the timing of geologic events: Geochimica et Cosmochimica Acta, v. 69, p. 475–483, doi: 10.1016/j.gca.2004.07.001.

Hintze, L.F., 1993, Geologic History of Utah: Brigham Young University Geology Studies Special Publication 7, 202 p.

Hintze, L.F., Willis, G.C., Laes, D.Y.M., Sprinkel, D.A., and Brown, K.D., 2000, Digital Geologic Map of Utah: Utah Geological Survey, scale 1:500,000, http://geology.utah.gov/maps/geomap/statemap/index.htm (2007).

IAEA (International Atomic Energy Agency), 2001, GNIP Maps and Animations: International Atomic Energy Agency, Vienna: http://isohis.iaea.org (2007).

IPCC (International Panel on Climate Change), 2005, Carbon dioxide capture and storage, *in* Metz, B., Davidson, O., de Coninck, H., Loos, M., and Meyer, L., eds., Carbon Dioxide Capture and Storage: New York, Cambridge University Press, 431 p.

Javoy, M., Pineau, F., and Delorme, H., 1986, Carbon and nitrogen isotopes in the mantle: Isotopes in geology; Picciotto volume: Chemical Geology, v. 57, p. 41–62, doi: 10.1016/0009-2541(86)90093-8.

Jenden, P.D., Hilton, D.R., Kaplan, I.R., and Craig, H., 1993, Abiogenic hydrocarbons and mantle helium in oil and gas fields; The future of energy gases: U.S. Geological Survey Professional Paper, Report P-1570, 31–56 p.

Kansas Geological Survey, 2003, Carbon dioxide solubility in water: Kansas Geological Survey Open-File Report 2003–33, 3 p. (http://www.kgs.ku.edu/PRS/publication//2003/ofr2003-33/) (2007).

Liu, Z., Zhang, M., Li, Q., and You, S., 2003, Hydrochemical and isotope characteristics of spring water and travertine in the Baishutai area (SW China) and their meaning for paleoclimate reconstruction: Environmental Geology, v. 44, p. 698–704, doi: 10.1007/s00254-003-0811-4.

Lollar, B.S., Ballentine, C.J., and O'Nions, R.K., 1997, The fate of mantle-derived carbon in a continental sedimentary basin; integration of C/He relationships and stable isotope signatures: Geochimica et Cosmochimica Acta, v. 61, p. 2295–2307, doi: 10.1016/S0016-7037(97)00083-5.

Lund, W.R., Taylor, W.J., Pearthree, P.A., Stenner, H., Amoroso, L., and Hurlow, H., 2002, Structural development and paleoseismicity of the Hurricane fault, southwestern Utah and northwestern Arizona, *in* Lund, W.R., ed., Field Guide to Geologic Excursions in Southwestern Utah and Adjacent Areas of Arizona and Nevada: U.S. Geological Survey Open-File Report 02–172, p. 1–84.

McCrea, J.M., 1950, On the isotopic chemistry of carbonates and a palaeotemperature scale: Journal of Physical Chemistry, v. 18, p. 849–857, doi: 10.1063/1.1747785.

Moreira, M., Kunz, J., and Allegre, C.J., 1998, Rare gas systematics in popping rock; isotopic and elemental compositions in the upper mantle: Science, v. 279, p. 1178–1181, doi: 10.1126/science.279.5354.1178.

Nelson, S.T., 2000, A simple, practical methodology for routine VSMOW/SLAP normalization of water samples analyzed by continuous flow methods: Rapid Communications in Mass Spectrometry, v. 14, p. 1044–1046, doi: 10.1002/1097-0231(20000630)14:12<1044::AID-RCM987>3.0.CO;2-3.

Nelson, S.T., and Dettman, D., 2001, Improving hydrogen isotope ratio measurements for on-line Cr reduction systems: Rapid Communications in Mass Spectrometry, v. 15, p. 2301–2306, doi: 10.1002/rcm.508.

Odling, N.E., Harris, S.D., and Knipe, R.J., 2004, Permeability scaling properties of fault damage zones in siliciclastic rocks: Journal of Structural Geology, v. 26, p. 1727–1747, doi: 10.1016/j.jsg.2004.02.005.

O'Nions, R.K., and Oxburgh, E.R., 1988, Helium, volatile fluxes and the development of continental crust: Earth and Planetary Science Letters, v. 90, p. 331–347, doi: 10.1016/0012-821X(88)90134-3.

Parkhurst, D.L., and Appelo, C.A.J., 1999, User's Guide to PHREEQC (Version 2)—A Computer Program For Speciation, Batch-Reaction, One-Dimensional Transport, and Inverse Geochemical Calculations: U.S. Geological Survey Water-Resources Investigations Report 99–4259, 310 p.

Portier, S., and Rochelle, C., 2005, Modelling CO_2 solubility in pure water and NaCl-type waters from 0 to 300 °C and from 1 to 300 bar: Application to the Utsira Formation at Sleipner: Chemical Geology, v. 217, p. 187–199, doi: 10.1016/j.chemgeo.2004.12.007.

Reid, M.R., and Graham, D.W., 1996, Resolving lithospheric and sub-lithospheric contributions to helium isotope variations in basalts from the Southwestern US: Earth and Planetary Science Letters, v. 144, p. 213–222, doi: 10.1016/0012-821X(96)00166-5.

Sanchez, A., 1995, Mafic Volcanism in the Colorado Plateau/Basin and Range Transition Zone, Hurricane, Utah [M.S. thesis]: Las Vegas, University of Nevada, Las Vegas, 92 p.

Sherwood Lollar, B., Ballentine, C.J., and O'Nions, R.K., 1997, the fate of mantle-derived carbon in a continental sedimentary basin: Integration of C/He relationships and stable isotope signatures: Geochimica and Cosmochimica Acta, v. 61, no. 11, p. 2295–2308.

Shipton, Z.K., Evans, J.P., Robeson, K., Forster, C.B., and Snelgrove, S., 2002, Structural heterogeneity and permeability in faulted eolian sandstone: Implications for subsurface modelling of faults: The American Association of Petroleum Geologists Bulletin, v. 86, p. 863–883.

Shipton, Z.K., Evans, J.P., Dockrill, B., Heath, J., Williams, A., Kirchner, D., and Kolesar, P.T., 2005a, Natural leaking CO_2-charged systems as analogs for failed geologic sequestration reservoirs, *in* Thomas, D., and Benson, S.M., eds., Carbon Dioxide Capture for Storage in Deep Geologic Formations—Results from the CO_2 Capture Project, Volume 2: London, Elsevier Science, p. 699–712.

Shipton, Z.K., Evans, J.P., and Thompson, L.B., 2005b, The geometry and thickness of deformation band fault core, and its influence on sealing characteristics of deformation band fault zones, *in* Sorkhabi, R., and Tusuji, Y., eds., Faults, Fluid Flow and Petroleum Traps: American Association of Petroleum Geologists Memoir 85, p. 181–195.

Stewart, M.E., Taylor, W.J., Pearthree, P.A., Solomon, B.J., and Hurlow, H.A., 1997, Neotectonics, fault segmentation, and seismic hazards along the Hurricane fault in Utah and Arizona: An overview of environmental factors in an actively extending region in Mesozoic to Recent Geology of Utah: Geological Society of America Field Trip Guide Book, 1997 Annual Meeting, Salt Lake City, Utah, and Brigham Young University Geology Studies, v. 42, pt. 2, p. 235–254.

Taylor, W.J., Stewart, M.R., and Orndorff, R.L., 2001, Fault segmentation and linkage: Examples from the Hurricane fault, Southwestern U.S.A., *in* Faulds, J.E., Bartley, J.M., and Rowley, P.D., eds., The geologic transition, high plateaus to Great Basin—A symposium and field guide: Utah Geological Association Publication 30, p. 113–126.

Valley, J.W., 2001, Stable isotope thermometry at high temperatures: Stable isotope geochemistry: Reviews in Mineralogy and Geochemistry, v. 43, p. 365–413, doi: 10.2138/gsrmg.43.1.365.

Zhou, Z., Ballentine, C.J., Kipfer, R., Schoell, M., and Thibodeaux, S., 2005, Noble gas tracing of graoundwater/coalbed methane interaction in the San Juan Basin, USA: Geochimica and Cosmochimica Acta, v. 69, no. 23, p. 5413–5428.

Manuscript Received 3 July 2007
Revised Manuscript Received 25 March 2008
Manuscript Accepted 12 May 2008

Printed in the U.S.A.